Eurasian Journal of Physics and Functional Materials

2023, 7(1), 60-72

Thermal and electrical properties of nanocrystalline superionic $Na_xCu_{1.75}S$ (x=0.1, 0.15, 0.2, 25) compounds

M.M. Kubenova*,[1], K.A. Kuterbekov[1], M.Kh. Balapanov[2], R.Kh. Ishembetov[2], B.M. Akhmetgaliev[2], A.M. Kabyshev[1], K.Zh. Bekmyrza[1], M.Kh. Zeleev[3], R.Sh. Palymbetov [1], B.U. Baikhozhaeva[1]

[1]L.N. Gumilyov Eurasian National University, Astana, Kazakhstan

[2]Bashkir State University, Ufa, Bashkortostan, Russia

[3]Bashkir State Medical University, Ufa, Bashkortostan, Russia

E-mail: kubenova.m@yandex.kz

DOI: **10.32523/ejpfm.2023070105**
Received: 10.03.2023 - after revision

The paper presents the results of the studies of thermal properties of nanocrystalline superionic $Na_xCu_{1.75}S$ (x=0.1, 0.15, 0.2, 25) compositions, and preliminary results of $Na_{0.1}Cu_{1.75}S$ using as energy stored cathode material in Na-ion half-cell with $NaPF_6$ electrolyte and Na anode. The compositions contain a few copper sulfide phases: monoclinic chalcocite Cu_2S, orthorhombic anilite $Cu_{1.75}S$, triclinic roxbyite $Cu_{1.74\div1.82}S$, also the compositions can contain monoclinic $Na_2Cu_4S_3$, orthorhombic Na_2S, cubic Cu_2O as inclusion phases. The sizes of powder particles lie in the range from 10 to 113 nm. Differential scanning calorimetry revealed in $Na_{0.1}Cu_{1.75}S$ the endothermic thermal effects with critical temperatures near 123 ° C, 42 ° C and 442 ° C, caused by structural transitions in copper sulfide. Fourth endothermic peak at 323 ° C presumably belongs to Na_2S phase. The minimum for the Fermi level at about 420 ° C is found with using of the e.m.f. E of the electrochemical cell of the $Cu/CuBr/Na_{0.10}Cu_{1.75}S/Pt$, which corresponds to minimum for the carrier concentration. This conclusion correlates well with the observed conductivity minimum at about 410 ° C. Electrode material $Na_{0.10}Cu_{1.75}S$ achieved a significant specific energy density 146.5 mAh/g in half-cell assembled from the cathode active material, electrolyte ($NaPF_6$ in 0.5 mol PC) and Na anode.

Keywords: thermoelectric materials; copper sulfide; crystal structure; conductivity; diffusion; thermal conductivity; Seebeck coefficient; superionic conductors

Introduction

Nanocrystalline copper sulfides and selenides have a wide range of applications due to their interesting and varied physical properties: for example, solar cells [1, 2], nanosized switches [3], photoluminescence sensors of barely visible impact damage [4], photoluminescence gas and humidity sensors [5], sensors of vapors of some organic compounds [6], plasmonic applications in synergistic therapies of near–infrared rays and magnetic resonance imaging [7], catalysts [8, 9], materials for photothermal therapy [10] and cetera. The most attractive, in our opinion, are the thermoelectric and electrochemical applies [11, 12]. In both cases, electronic, ionic, and phonon transport play important roles, and the influence of various physical and chemical factors, as methods and conditions of synthesis, particle sizes and shapes, surface conditions, the presence of impurities ets. is very essential. In this article, we will continue the study of nanocrystalline sodium–containing copper sulfides obtained by the reaction method in an alkaline melt.

In works [13, 14] were presented the results of studies of $Na_{0.05}Cu_{1.95}S$, $Na_{0.075}Cu_{1.925}S$, $Na_{0.10}Cu_{1.90}S$, $Na_{0.125}Cu_{1.750}S$, $Na_{0.15}Cu_{1.85}S$, $Na_{0.17}Cu_{1.80}S$, $Na_{0.20}Cu_{1.77}S$ compositions. The alloys were heterophasic and contained such copper sulfide phases as digenite Cu_9S_5, copper disulfide CuS_2, covellite CuS, anilite Cu_7S_4 in various combinations. A quasi-one-dimensional $Na_2Cu_4S_3$ phase was detected too in the composition of the $Na_{0.20}Cu_{1.77}S$ alloy. It was obtained that the electronic conductivity of the nanocrystalline alloys are two orders of magnitude lower than in isolated pure Cu_9S_5, CuS_2, CuS, Cu_7S_4 phases, from which the alloys consist. The reason for the low conductivity of the alloys was assumed to be the presence of weakly conducting interfacial layers and sodium doping of non-stoichiometric phases Cu_9S_5 ($Cu_{1.8}S$) and Cu_7S_4 ($Cu_{1.75}S$), leading to the compensation of holes by electrons of impurity sodium atoms. Due to the low thermal conductivity near 0.2 $Wm^{-1}K^{-1}$, a rather high dimensionless thermoelectric figure of merit $ZT \approx 0.28$ at 570 K was obtained for the $Na_{0.15}Cu_{1.85}S$ composition. In the work [15] crystal structure and thermoelectric properties were investigated for $Na_{0.3}Cu_{1.6}S$, $Na_{0.35}Cu_{1.5}S$, $Na_{0.4}Cu_{1.55}S$ nanocrystalline compositions. For the $Na_{0.4}Cu_{1.55}S$ sample, a high value of ZT=0.84 was obtained at 358 °C.

Materials with a low content of sodium in copper sulfide, within the region of solid solubility, turned out to be more successful for thermoelectric applies. In work [16] Z.H. Ge et al described the thermoelectric properties of bulk samples of $Na_xCu_9S_5$ copper sulfide (x=0, 0.025, 0.05, 0.15, 0.25), consolidated using spark plasma sintering technology from nanopowder and the solubility of sodium in the crystal structure of copper sulfide to a composition of x=0.05 was revealed. The presence of many nanoscale pores and grains was found, which led to a decrease in thermal conductivity by a factor of 2–3. As a result, they achieved a high value of ZT=1.1 at 500 °C for $Na_{0.05}Cu_9S_5$, mainly due to a decrease in thermal conductivity. At a higher sodium concentration (as for the $Na_{0.25}Cu_9S_5$ alloy), the formation of inclusions of the Na_2S and $Cu_{1.96}S$ phases was noted. Latter the porous $Cu_{1.8}S$ based composites with Na_2S polycrystalline bulk samples were prepared via the incorporation of mechanical alloying and spark plasma

sintering technique by employing $Na_2S \cdot 9H_2O$ as a addictive, and a peak ZT value of 0.78 at 500 °C has been obtained for the $Cu_{1.8}S$ bulk specimen with 2 wt% Na_2S impurity, which enhances by 160% in comparison with the pure $Cu_{1.8}S$ (0.49 at °C) [17].

Copper chalcogenides have already shown themselves to be promising materials for NIBs too [18–23]. Heterogeneous structured–metal sulfides are widely used in various applications due to their excellent electrochemical activity. H.Park et al. [21] reported a facile synthesis of $Cu_{1.75}S/Cu_{1.8}S$ microspheres assembled with mesoporous nanosheets and their application in sodium-ion batteries. It is revealed that roxbyite $Cu_{1.75}S$ is transformed into a digenite $Cu_{1.8}S$ phase without a significant morphological change by a thermal treatment. Remarkable sodium storage properties were achieved, including charge capacity 327 mAh g^{-1} at 0.1 C, high–rate capabilities of 285 (88%) and 290 mAh g^{-1} (90%) at 3 C in a voltage range of 0.3–2.1 V versus Na/Na^+.

Investigation of the $Cu_{1.8}S/C$ composite material as the negative electrode active material in combination with a concentrated electrolyte composed of a 3.3 m solution of sodium bis(fluorosulfonyl)imide (NaFSI) in trymethyl phosphate and fluoroethylene carbonate (FEC) as the additive is reported by H. Li et al. [22]. Such a combination enables the stable cycling of the conversion–type $Cu_{1.8}S/C$ electrode material for hundreds of cycles with high capacity (380 $mA \cdot h \cdot g^{-1}$). A full cell using the $Na_3V_2(PO_4)_3$ /C cathode and a $Cu_{1.8}S$ anode also demonstrates stable cycling performance for 200 cycles with a promising Coulombic efficiency (CE) (99.3%). A concentrated TMP electrolyte using NaFSI salt and FEC additive enables stable cycling of the $Cu_{1.8}S/C$ anode, with high reversible capacity and rate performance. The excellent electrochemical performance is enabled by the NaF–rich SEI derived from both the salt and the FEC additive.

Ionic conductivity in sodium-doped copper sulfide $Na_{0.2}Cu_{1.8}S$ was recently reported in the study [24], in which it was noted that doping with sodium did not significantly affect the ionic conductivity of copper sulfide: the ionic conductivity increase exponentially up 1.5 to 2.3 S cm^{-1} in the temperature range up 630 to 690 K. Observed values are comparable with the level of the ionic conductivity of the binary copper sulfide. Results of studies of chemical diffusion and ionic conductivity in $Na_xCu_{1.75}S$ (x=0.1, 0.15, 0.2, 25) nonstoichiometric nanocrystalline superionic materials were reported recently by K. Kuterbekov et al. [25]. High values of the coefficient of conjugated chemical diffusion of cations and electronic holes ($1.1 \cdot 10^{-3}$ and $1.65 \cdot 10^{-3}$ cm^2/s at 410 °C) were observed in the $Na_{0.10}Cu_{1.75}S$ and $Na_{0.20}Cu_{1.75}S$ electron-ionic conductors. Activation energies of the total ionic conductivity are measured as 0.30 and 0.40 eV for superionic $Na_{0.10}Cu_{1.75}S$ and $Na_{0.15}Cu_{1.75}S$ phases respectively. In the superionic phases the measured values of the total ionic conductivity are 2.8, 1.5 and 2.0 S/cm for $Na_{0.10}Cu_{1.75}S$, $Na_{0.15}Cu_{1.75}S$ and $Na_{0.20}Cu_{1.75}S$ at 410 °C respectively. Thus, it was conclude in [25] that insertion of sodium to copper sulfide not lead to worse of high ionic conductivity in the superionic phase. In this article, we present the results of the studies of thermal properties of nanocrystalline superionic $Na_xCu_{1.75}S$ (x=0.1, 0.15, 0.2, 25) compositions, and preliminary results of $Na_{0.1}Cu_{1.75}S$ using as energy stored cathode material in

Na-ion half-cell with $NaPF_6$ electrolyte and Na disc anode.

Materials and methods

The synthesis of the $Na_xCu_{2-x-y}S$ powders was carried out by reaction of CuCl with $Na_2S \cdot 9H_2O$ in a melt of NaOH and KOH hydroxides. Details of synthesis procedure are described in our earlier paper [25].

From the powders the tablets were prepared in the form of $2 \cdot 5 \cdot 20$ mm^3 for measuring of the transport properties. Cold pressing under pressure of 2–3 tons/cm^2 was used. After pressing the annealing for 8 hours at 450 °C in an argon atmosphere was provided for all samples.

X-ray phase analysis of the samples was carried out on a Bruker diffractometer (Germany) using radiation using CuKα X-ray tube radiation and a graphite monochromator with a diffracted beam. Images of the powder particles were obtained with using of scanning electron microscope (SEM) MIRA3 from TESCAN. The study of phase transitions and heat capacity (c_p) measurements in $Na_xCu_{1.75}S$ samples was carried out by differential scanning calorimetry method (DSC) with DSC 404 F1 Pegasus instrument (NETZSCH, Germany) in an argon atmosphere in the temperature range of 30–600 °C. The heating rate was 10 K/min.

The thermal diffusivity (D) was measured by the laser flash method with LFA 467 HT HyperFlash device (NETZSCH, Germany) in argon atmosphere. The thermal conductivity was calculated as $k = \rho D c_p$. The sample densities ρ to determine thermal conductivities were measured using the sample's volume and mass.

Mixed type of conductivity of the studied materials does not allow the use of conventional methods of conductivity measuring, so the electronic conductivity was measured by well-known method of suppressing of ionic current component, described, for example, in [26, 27]. To separate the electronic conductivity, the ionic current component was suppressed by Pt electrodes and potential probes.

A constant electron current of 10 mA was passed through the $Na_{0.1}Cu_{1.75}S$ sample using graphite inert electrodes until a steady state was established. Steady potential difference U_{ii}^{∞} between two Pt electronic probes was used to calculate the electronic conductivity σ_e.

$$\sigma_e = \frac{Il}{(U_{ee}^{\infty} - U_{ee}^{0})S}, \quad (1)$$

where I is the electron current, l is the distance between Pt electronic probes, S is a cross square of a sample, U_{ee}^{0} is the initial potential difference between Pt electronic probes before turn on the current. For measurements of electronic Seebeck coefficient Wagner's method [28] was used. Temperature gradient about 10 K/cm was kept for the measurement time. Chromel branches of the chromel-alumel thermocouples were used as electronic potential probes for measurement of the electronic thermoelectric e.m.f. at steady state after electronic current switching off.

The measurement error for conductivity did not exceed 3–5%, for Seebeck coefficient it was in range of 4–7%. The error in measuring of the thermal conductivity was 7–10%.

The measurements were performed in inert atmosphere of purified argon.

Results and discussion

X-ray phase analysis, electron microscopy and differential scanning calorimetry

The results of X-ray phase analysis of the $Na_{0.15}Cu_{1.75}S$, $Na_{0.20}Cu_{1.75}S$ and $Na_{0.25}Cu_{1.75}S$ samples were described in our recent work [18], except for the $Na_{0.10}Cu_{1.75}S$ sample. For example, the powder X-ray diffraction pattern of the $Na_{0.15}Cu_{1.75}S$ sample taken at room temperature is shown in Figure 1 a. This alloy contains next phases: triclinic roxbyite, orthorhombic anilite, monoclinic $Na_2Cu_4S_3$, cubic Cu_2O. Analysis of the spectrum of Figure 1 a revealed that the main phase of $Na_{0.15}Cu_{1.75}S$ sample is the triclinic roxbyite $Cu_{1.8125}S$ with space group P and cell parameters, a=13.4051(9) Å, b=13.4090(8) Å, c=15.4852(3) Å, $\alpha = 90.022(2)^\circ$, $\beta = 90.021(2)^\circ$, $\gamma = 90.020(3)^\circ$.

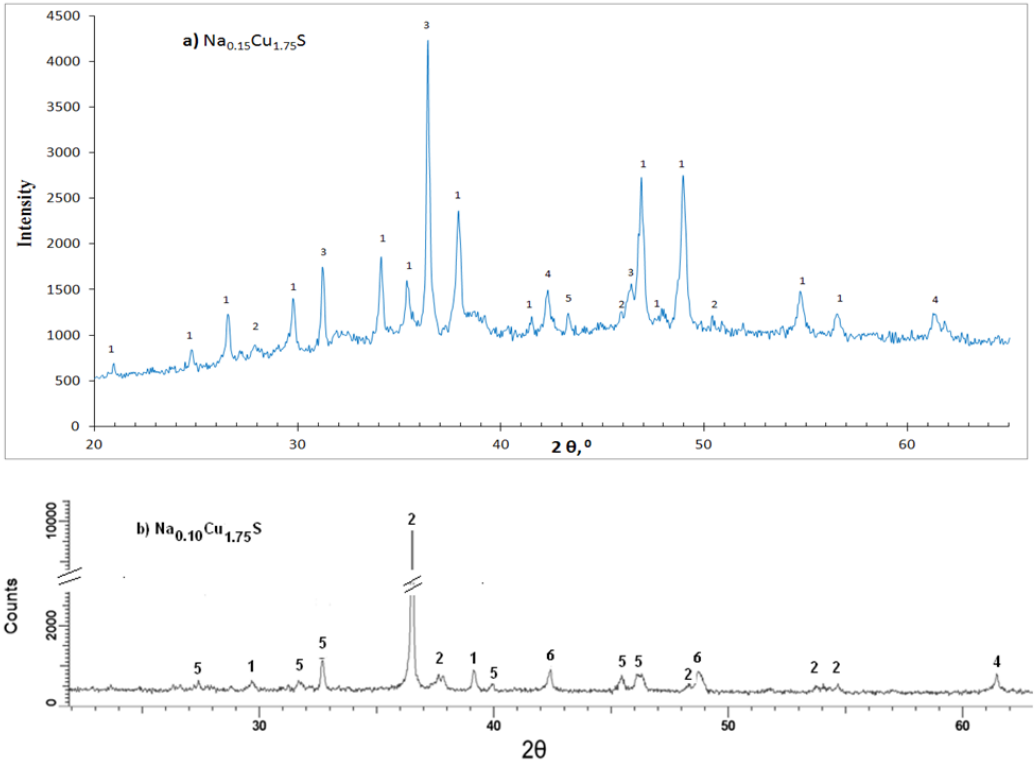

Figure 1. Powder diffraction pattern of of the $Na_{0.15}Cu_{1.75}S$ (a), $Na_{0.10}Cu_{1.75}S$ (b) samples taken at room temperature. Digits above pikes denotes: 1–triclinic roxbyite, 2–orthorhombic anilite, 3–monoclinic $Na_2Cu_4S_3$, 4–cubic Cu_2O, 5–monoclinic chalcocite Cu_2S, 6–orthorhombic Na_2S.

Roxbyite is a phase of variable composition with the formula $Cu_{1.74\div1.82}S$. The structure of roxbyite is based on a hexagonal-close-packed framework of sulfur atoms with the copper atoms occupying these layers, all having triangular

coordination. The crystal structure of roxbyite bears a strong kinship to those of low chalcocite and djurleite.

Along with the main phase, the studied $Na_{0.15}Cu_{1.75}S$, $Na_{0.20}Cu_{1.75}S$ and $Na_{0.25}Cu_{1.75}S$ samples contain orthorhombic anilite $Cu_{1.75}S$, monoclinic chalcocite Cu_2S, and as impurity the cubic copper oxide Cu_2O. The sizes of crystallites, estimated from the half-width of X-ray lines by the Williamson-Hall method, lie in the range from 13 to 82 nm in $Na_{0.15}Cu_{1.75}S$ alloy, from 10 to 113 nm in $Na_{0.20}Cu_{1.75}S$ alloy and from 13 to 99 nm in $Na_{0.25}Cu_{1.75}S$ alloy which is due to approximately the same conditions for the synthesis in the melt of sodium and potassium hydroxides.

The powder X-ray diffraction pattern of the $Na_{0.10}Cu_{1.75}S$ sample taken at room temperature is shown in Figure 1 b. This alloy contains next phases: triclinic roxbyite (a=13.3870 Å, b=13.3950 Å, c=15.4810 Å; $\alpha = 89.800^\circ$, $\beta = 89.980^\circ$, $\gamma = 90.080^\circ$), orthorhombic anilite (a=7.8900 Å, b=7.8400 Å, c=11.0100 Å; $\alpha = 90.000^\circ$, $\beta = 90.000^\circ$, $\gamma = 90.000^\circ$), prevailing phase is monoclinic chalcocite Cu_2S (a=15.2460 Å, b=11.8840 Å, c=13.4940 Å, $\alpha = 90.000^\circ$, $\beta = 116.350^\circ$, $\gamma = 90.000^\circ$), orthorhombic Na_2S (a=6.7070 Å, b=4.1200 Å, c=8.0250 Å; $\alpha = 90.000^\circ$, $\beta = 90.000^\circ$, $\gamma = 90.000^\circ$), impurity cubic Cu_2O (a=4.2696 Å).

For $Na_{0.10}Cu_{1.75}S$ powder the sizes of particles estimated from the half–width of X-ray lines lie in the range from 24 to 104 nm.

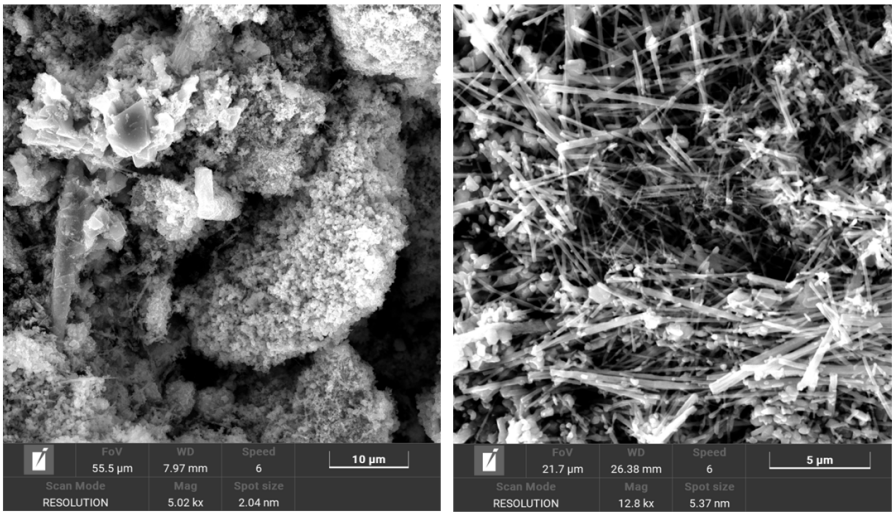

a) b)

Figure 2. Image of the $Na_{0.10}Cu_{1.75}S$ powder taken with MIRA3 TESCAN scanning electron microscope. On Figure 2 a, with the width of the field of view of 55 µm the big Cu_2S agglomerates of round or block forms contained nanosized particles are visible mainly. Figure 2 b shows a surface area with nanostrips or nanowires of anilite.

Figure 2 shows a snapshot of the powder $Na_{0.10}Cu_{1.75}S$ sample. On Figure 2 a, with the width of the field of view of 55 µm the big Cu_2S agglomerates of round or block forms contained nanosized particles are visible mainly. Figure 2 b shows a surface area with nanostrips or nanowires of anilite. The particle sizes according to electron microscopy exceed by several times the estimated results from the X-ray line half-width. Perhaps this difference is due to the presence of subblocks inside the particles, due to which the estimate from the X-ray line half-width gives smaller sizes.

In Figure 3 the differential scanning calorimetry curve for $Na_{0.10}Cu_{1.75}S$ sample is presented. The DSC curve demonstrate endothermic thermal effect at 123 ° C and double endothermic peak at 422 and 442 ° C. Rather intensive peak are observed at 323 ° C too.

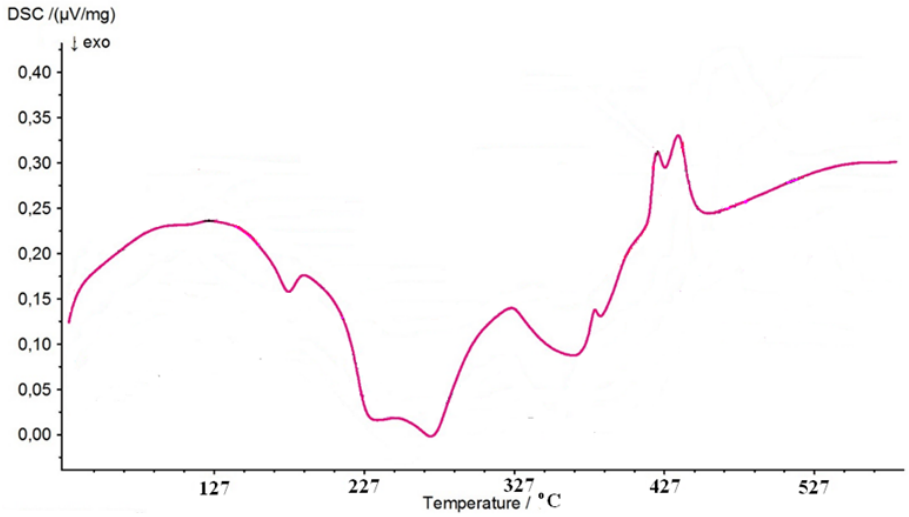

Figure 3. Curve of differential scanning calorimetry of $Na_{0.10}Cu_{1.75}S$ sample recorded in argon atmosphere.

In our opinion, a wide (with a width of 30–60 ° C) phase transition centered at 123 ° C can be considered as a structural transition to the superionic hexagonal phase of copper sulfide, the temperature of which depends on the stoichiometry of the composition [29]. It is delayed by 20 degrees relative to the transition point for coarse-grained copper sulfide, which can be attributed to nanosizes of crystallites. The second strong thermal effect at 422 and 442 ° C is close to the transition point from the hexagonal to the cubic form of pure copper sulfide (437 ° C [30]).

The thermal effect at 323 ° C, perhaps, is caused by phase transition in the orthorhombic Na_2S phase. A transition temperature of $\approx$320 ° C for Na_2S was reported by E.K. Ovechkin et al. [31].

Electron transfer

Figure 4 presents experimental temperature dependences of electronic conductivity (a), Seebeck coefficient (b), and power factor (c) for $Na_{0.10}Cu_{1.75}S$ sample. Phase transitions corresponding to thermal effects on the DSC curves in Figure 3 also appeared as peaks in the temperature dependences of Figure 4. The conductivity shows maxima around 100 ° C, 315 ° C, and a minimum near 420 ° C. The Seebeck coefficient behaves in antiphase with respect to the conductivity: the minima occur at about 80 ° C, 300 ° C, the maximum is observed at about 415 ° C. The $Na_{0.10}Cu_{1.75}S$ composition demonstrate a properties of degenerate semiconductor exclude three short intervals in which an activation character of the conductivity is observed (the activation energy values are 0.067 eV, 0.19 eV and 2.7 eV for the temperature ranges correspondingly: from 53 to 84 oC, from 254 to 303 ° C, and from 405 to 445 ° C). For low temperature regions the same activation energy value (0.067 eV) for $Na_{0.075}Cu_{1.925}S$ alloy and 0.057 eV for

$Na_{0.05}Cu_{1.95}S$, $Na_{0.10}Cu_{1.90}S$, $Na_{0.125}Cu_{1.75}S$ were reported earlier [32, 33]. For the low-temperature copper sulfide phase (djurleite $Cu_{1.92}S$), Sorokin G.P. and Paradenko A.P. [34] reported an activation energy of 0.09 eV.

Thermal conductivity of $Na_{0.10}Cu_{1.75}S$ composition (Figure 5, curve 4) generally follows the Wiedemann-Franz law, and there is a correspondence between the temperature change in the conductivity in Figure 4 and the thermal conductivity in Figure 5. However, there are deviations from the Wiedemann-Franz law: in the range between 100 and 200 °C, the thermal conductivity remains approximately constant, although the electronic conductivity decreases by half; similarly, in the range from 300 to 400 °C, the conductivity drops by almost 10 times, while the thermal conductivity remains practically unchanged. It was noticed also in work [16] by Ge et al., that the equation $\kappa_{carrier} = L\sigma T$, where L is Lorenz number, σ is electrical conductivity, may be unsuitable for such superionic conductors as $Cu_{1.8}S$.

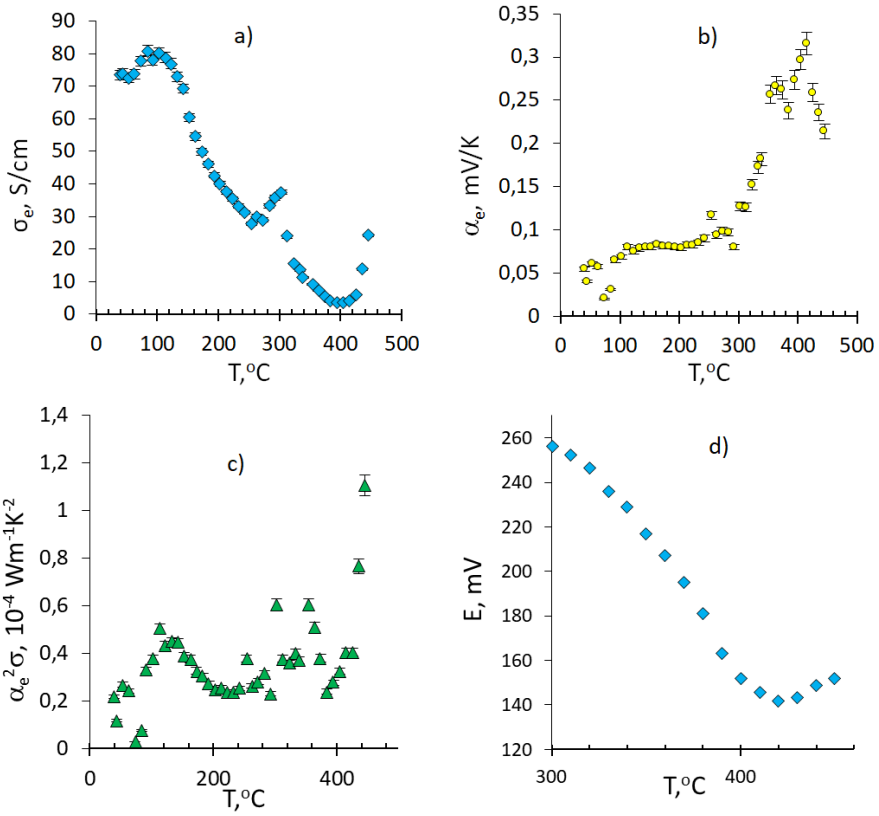

Figure 4. Temperature dependences of electronic conductivity (a), Seebeck coefficient (b) and power factor P= $\alpha_e^2\sigma$ (c) for $Na_{0.10}Cu_{1.75}S$ sample. Electromotive force of $Cu/CuBr/Na_{0.10}Cu_{1.75}S/Pt$ electrochemical cell is shown as function of temperature in figure (d).

Electromotive force (e.m.f.) of $Cu/CuBr/Na_{0.10}Cu_{1.75}S/Pt$ electrochemical cell is shown as function of temperature in Figure 4 d.

Due to the strong structural disorder of the superionic phase, the chemical potential of cations can be considered constant with small changes in their concentration, and in this case, the e.m.f. E of an electrochemical cell of the $Cu/CuBr/Na_{0.10}Cu_{1.75}S/Pt$ type is the height of the Fermi level μ in the phase relative to the Fermi level μ^0_{Cu} in the metal reference electrode (Cu) [12, 32].

$$\mu = \mu^0_{\mathrm{Cu}} + eE, \tag{2}$$

We see in Figure 4 d that at about 420 °C there is a minimum for the Fermi level and, accordingly, for the carrier concentration. This conclusion correlates well with the observed conductivity minimum at about 410 °C in Figure 4 a.

Temperature dependence of power factor $P = \alpha_e^2\sigma$ for $Na_{0.10}Cu_{1.75}S$ sample is presented in Figure 4 c. Figure 4 c shows an increase in the thermoelectric power factor during a phase transition from the low-temperature phase to the hexagonal phase (weak maximum near 110 °C) and at the phase transition from the hexagonal phase to the cubic phase (sharp peak near 440 °C). Also local peak at 300 °C vicinity is observed, which is probably caused by phase transition in Na_2S phase of the composition.

The low conductivity, presumably caused by the presence of Cu_2O and Na_2S dielectric phases, did not allow obtaining high values of thermoelectric power and efficiency of the material. The considerable value of thermoelectric figure of merit ZT=0.13 for $Na_{0.10}Cu_{1.75}S$ sample was observed at 400 °C.

Thermal properties

The curves in Figure 5 have approximately the same character: from room temperature to ≈200–210 °C, a plateau is observed, then from 200–230 °C to ≈310–320 °C, a sharp decrease in thermal conductivity follows, and then there is again an area of weak changes in thermal conductivity. The drop of the thermal conductivity is partly due to the decrease in electronic conductivity, a strong decreasing in thermal diffusivity was observed in this temperature range also.

Curve 5 in Figure 5 is plotted for multiphase $Na_{0.05}Cu_{1.8}S$ sample, contained Na_2S and $Cu_{1.96}S$ inclusions in addition to main $Na_{0.03}Cu_{1.8}S$ phase, according to data Z.-H. Ge [16]. The character of the dependence is similar to that obtained for our samples $Na_xCu_{1.75}S$ (x=0.1, 0.15, 0.2, 25), which also contain few superionic phases-roxbyite $Cu_{1.8125}S$, anilite $Cu_{1.75}S$, chalcocite Cu_2S, and Na_2S. The curve 4 of the thermal conductivity for $Na_{0.10}Cu_{1.75}S$ lies lower than the curve of Z.-H. Ge for $Na_{0.05}Cu_{1.8}S$ sample. However, in general, the values of the thermal conductivity for our samples turned out to be unexpectedly high, inconsistent with the rather low values of the electronic conductivity. In the work of Z.-H. Ge the electronic conductivity of the samples is at least 10 times higher, the content of sodium impurity in the lattice, which reduces thermal conductivity, is also 10 times lower than that of our samples, but the thermal conductivity of our $Na_{0.15}Cu_{1.75}S$ and $Na_{0.25}Cu_{1.75}S$ samples in the temperature range from 30 up to 300 °C turned out to be higher than even that of pure $Cu_{1.75}S$. The reasons for this behavior of thermal conductivity are unclear and require further study.

Electrochemical studies

The sample $Na_{0.10}Cu_{1.75}S$ was crushed and grinded in mortar. In the next step, the slurry was prepared from powder of active material ($Na_{0.10}Cu_{1.75}S$), acety-

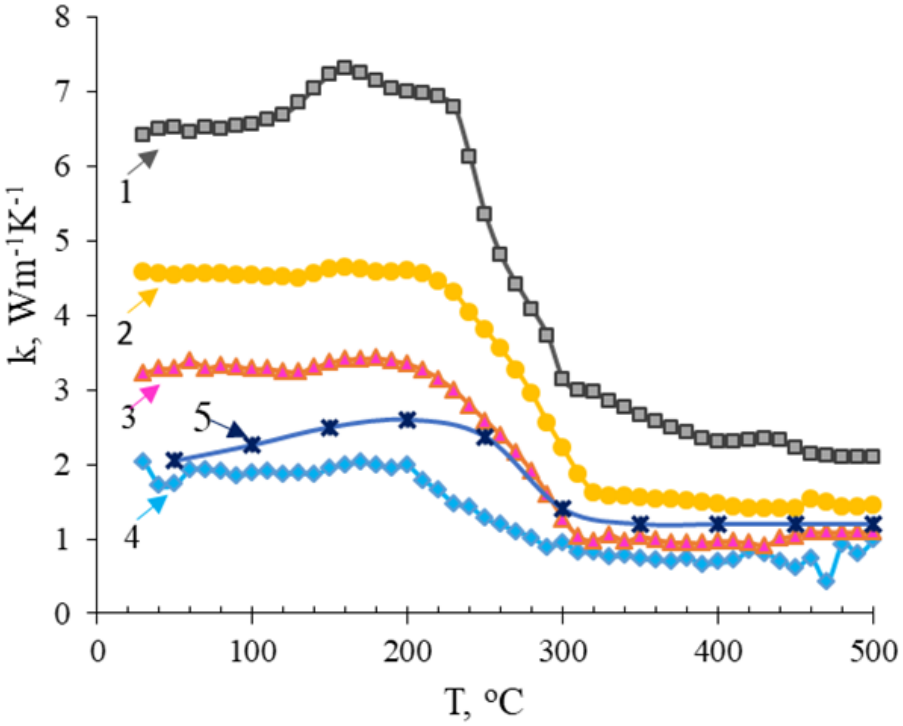

Figure 5. Temperature dependences of the thermal conductivity for $Na_{0.10}Cu_{1.75}S$ (curve 4), $Na_{0.15}Cu_{1.75}S$ (1), $Na_{0.20}Cu_{1.75}S$ (3) and $Na_{0.25}Cu_{1.75}S$ (2) samples. Curve 5 is plotted for multiphase $Na_{0.05}Cu_{1.8}S$ sample, contained Na_2S and $Cu_{1.96}S$ inclusions in addition to main $Na_{0.03}Cu_{1.8}S$ phase, according to data Zhen-Hua Ge [16].

lene black, Polyvinylidene fluoride (PVDF) binder, and N-Methyl-2-Pyrrolidone (NMP) solvent (80:10:10 in ratio).

The battery (half-cell) was assembled from the cathode active material, separator (Whatman, GF/D), electrolyte ($NaPF_6$ in 0.5 mol PC: FEC (98:2)) and anode Na disc.

This half-cell was galvanstatically cycled on Neware battery tester, at cut-off voltage 1.0–3 V.

The operation of the battery is based on a reversible potential-forming reaction:

$$Na_xCu_yS + zNa^+ + ze^- \Leftrightarrow Na_{x+z}Cu_{yS}(x+z \prec 2, y \prec 2), \quad (3)$$

Cycling depth and battery capacity is determined by parameter z.

The results of cycling are shown in Figure 6. Maximum achieved specific gravity energy density 146.5 mAh/g. After the first recharge of the cell, the energy density is reduced to 130 mAh/g.

Charge-discharge curves of 5 cycles for the half-cell with energy stored electrode $Na_{0.10}Cu_{1.75}S$ are presented in Figure 6.

The sodium/copper sulfide (Na/Cu_2S) electrochemical system was studied by J.-S. Kim et al. [18] using the 1M $NaCF_3SO_3$-TEGDME electrolyte. The first discharge capacity was 294 mAh/g and decreased to 220 mAh/g after 20 cycles. Our trial studies gave rather lower results. One of the reasons for this seems to be the insufficiently high electronic conductivity of the sample. Another reason may be poor electrolyte selection. Also, the capacitance, of course, was reduced by the content of Cu_2O impurity. Of course, there may be other reasons also. To improve the battery cycleability, perhaps, it is necessary to add another

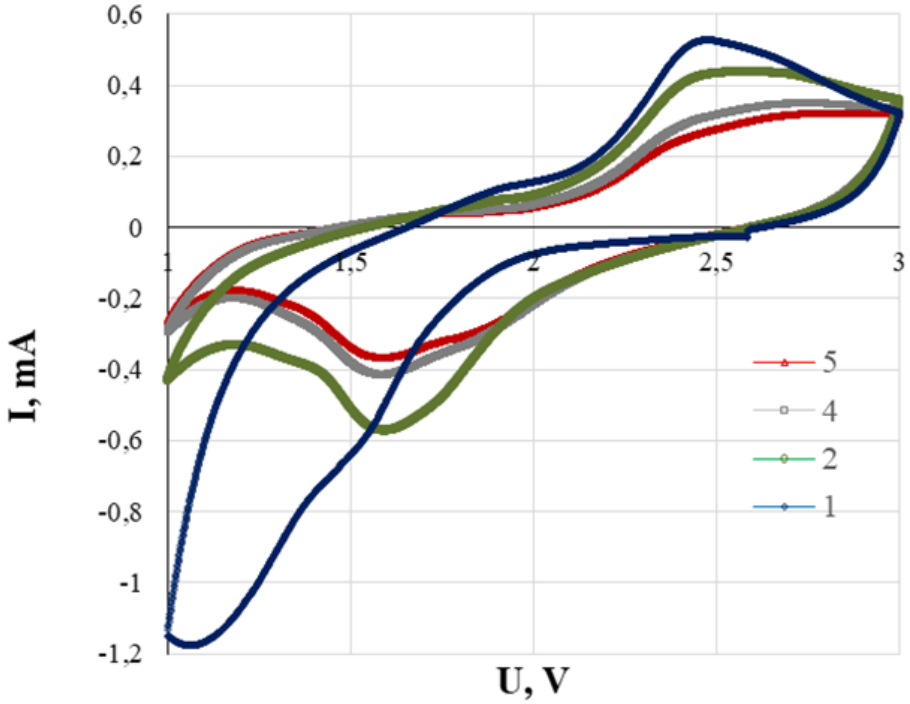

Figure 6. Charge-discharge curves of 5 cycles for the half-cell with energy stored $Na_{0.10}Cu_{1.75}S$ electrode. Third cycle is not shown.

carbon filler, to dampen mechanical stresses and keep the crystalline structure of the material intact during long-term cycling. Composite materials look more promising, using for example, a crumpled graphene, which increases both the capacity and the cycle life of the battery.

Conclusion

$Na_{0.10}Cu_{1.75}S$ alloy prepared by reaction of CuCl with $Na_2S \cdot 9H_2O$ in a melt of NaOH and KOH hydroxides possess complicated phase composition including monoclinic chalcocite Cu_2S (prevailing phase), orthorhombic anilite $Cu_{1.75}S$, triclinic roxbyite, orthorhombic Na_2S, impurity cubic Cu_2O. The sizes of particles estimated from the half-width of X-ray lines lie in the range from 24 to 104 nm for $Na_{0.10}Cu_{1.75}S$ powder. Differential scanning calorimetry revealed two endothermic thermal effects with critical temperatures near 123 °C and 422 °C, which caused by structural transitions in copper sulfide. Third endothermic peak at 323 °C presumably belongs to Na_2S phase of the alloy.

The low electronic conductivity in $Na_{0.10}Cu_{1.75}S$ may be due to the high content of the stoichiometric Cu_2S phase and the presence of dielectric phases Na_2S and Cu_2O. Low electronic conductivity causes low value of thermoelectric figure of merit ZT for $Na_{0.10}Cu_{1.75}S$ sample in investigated temperature range 20–400 °C, though Seebeck coefficient demonstrates values higher 0.1 mV/K and thermal conductivity have suitable small values from 0.8 to 1.1 $Wm^{-1}K^{-1}$ in temperature interval of 300–500 °C. The minimum for the Fermi level at about 420 °C is found with using of the e.m.f. E of the electrochemical cell of the $Cu/CuBr/Na_{0.10}Cu_{1.75}S/Pt$, which corresponds to minimum for the carrier

concentration. This conclusion correlates well with the observed conductivity minimum at about 410 °C. The thermal conductivity for $Na_{0.10}Cu_{1.75}S$ is observed lower than that for $Na_{0.05}Cu_{1.8}S$ sample of Z.-H. Ge [16], however, for other samples ($Na_{0.15}Cu_{1.75}S$, $Na_{0.20}Cu_{1.75}S$ and $Na_{0.25}Cu_{1.75}S$), the thermal conductivity turned out to be unexpectedly high, despite the weak conductivity and high sodium impurity concentration, which requires further consideration.

Electrode material on base of $Na_{0.10}Cu_{1.75}S$ powder achieved a considerable specific gravity energy density 146.5 $mA \cdot h/g$ in half-cell assembled from the cathode active material, electrolyte ($NaPF_6$ in 0.5 mol PC and Na disc anode. After the first recharge of the cell, the energy density is reduced to 130 $mA \cdot h/g$. One of the possible ways to increase the cycleability of the battery, we see the addition of a carbon filler, for example, crumpled graphene, to the cathode material in order to dampen mechanical stresses and keep the crystalline structure of the material intact during long-term cycling.

Acknowledgments

This research was funded by the Science Committee of the Ministry of Science and Higher Education of the Republic of Kazakhstan (No. AP14871197).

References

[1] G. Lakhotiya et al., Current Applied Physics **19**(4) (2019) 394-399. [*CrossRef*]
[2] X. Shuai et al., Nanoscale Research Letters **9** (2014) 513. [*CrossRef*]
[3] T. Tamura et al., Journal of Physics: Conference Series **61** (2007) 1157-1161. [*CrossRef*]
[4] F. Capezzuto et al., Composite Structures **92** (2010) 1913-1919. [*CrossRef*]
[5] J. Xu et al., Adv. Funct. Mater. **19** (2009) 1759-1766. [*CrossRef*]
[6] M.B. Muradov et al., Surface Engineering and Applied Electrochemistry **43** (2007) 512-515. [*CrossRef*]
[7] C. Coughlan et al., Chem. Rev. **117**(9) (2017) 5865-6109. [*CrossRef*]
[8] S. Li et al., ACS Catalysis **12**(15) (2022) 9074-9082. [*CrossRef*]
[9] N. Manivelan et al., ACS Applied Materials & Interfaces **14**(27) (2022) 30812-30823. [*CrossRef*]
[10] Y. Zhao et al., ACS Biomaterials Science & Engineering **6**(9) (2020) 4799-4815. [*CrossRef*]
[11] F.F. Jaldurgam et al., Nanomaterials **11**(4) (2021) 895. [*CrossRef*]
[12] M.M. Kubenova et al., Nanomaterials **11**(9) (2021) 2238. [*CrossRef*]
[13] M.K. Balapanov et al., Eurasian Journal of Physics and Functional Materials **2**(3) (2018) 231-241. [*CrossRef*]
[14] M.M. Kubenova et al., Eurasian Journal of Physics and Functional Materials **4**(1) (2020) 67-85. [*CrossRef*]
[15] M.Kh. Balapanov et al., Vestnik Bashkirskogo Universiteta **24**(4) (2019) 823-829. (in Russian) [*CrossRef*]
[16] Z.H. Ge et al., Advanced Energy Materials **6**(16) (2016) 1600607. [*CrossRef*]

[17] Y. Zhang et al., Materials Science in Semiconductor Processing **107** (2020) 104848. [*CrossRef*]
[18] J.-S. Kim et al., Journal of Power Sources **189** (2009) 864-868. [*CrossRef*]
[19] J.-L. Yue et al., Chem. Commun. **49** (2013) 5868-5870. [*CrossRef*]
[20] Yutao Jiang et al., CrystEngComm **24** (2022) 3355-3362. [*CrossRef*]
[21] H. Park et al., Crystal Growth & Design **20**(5) (2020) 3325-3333. [*CrossRef*]
[22] H. Li et al., Small structures **2**(8) (2021) 2100035. [*CrossRef*]
[23] R. Lu et al., Journal of Physics D: Applied Physics **55**(33) 334001. [*CrossRef*]
[24] M.Kh. Balapanov et al., Ionics **24**(5) (2018) 1349-1356. [*CrossRef*]
[25] K.A. Kuterbekov et al., Ionics **28** (2022) 4311-4319. [*CrossRef*]
[26] W. Weppner et al., Annual Review of Materials Science **8** (1978) 269-311. [*CrossRef*]
[27] I. Yokota, J. Phys. Soc. Jpn. **16** (1961) 2213-2223. [*CrossRef*]
[28] C. Wagner, Progr. in Sol. Chem. Phys. **7** (1972) 1-37.
[29] D.J. Chakrabarti et al., Bulletin of Alloy Phase Diagrams **4** (1983) 254-271. [*CrossRef*]
[30] F. Gronvold et al., J. Chem. Thermodyn. **19** (1987) 1183-1198.
[31] E.K. Ovechkin et al., J. Inorganic Chem. **16**(11) (1971) 1672-1674.
[32] S. Miyatani, J. Phys. Soc. Jpn. **34** (1973) 422-432. [*CrossRef*]
[33] M.M. Kubenova et al., IOP Conference Series: Material Science and Engineering **447** (2018) 012031. [*CrossRef*]
[34] G.P. Sorokin et al., Izvestiya Vuzov. Fizika (USSR) **5** (1966) 91-95. (In Russian)